©2016 Published in 4th International Symposium on Innovative Technologies in Engineering and Science 3-5 November 2016 (ISITES2016 Alanya/Antalya - Turkey)

Numerical and Analytical Investigations on The Stress Distributions in Single-Lap Joints

*[1]Özkan Öz and [2]Halil Özer
*[1]Industrial Design Engineering, Faculty of Technology, Karabuk University, Karabuk, Turkey
[2] Mechanical Engineering Department, Faculty of Mechanical Engineering, Yıldız Technical University, Istanbul, Turkey

Abstract:

The objective of this paper is to compare the shear and peel stress distributions in the single lap joints obtained using analytical model with those obtained using numerical analysis. The Zhao's closed form solution that includes the bending moment effect was used as an analytical model. In the numerical analysis, two dimensional finite element model with plane strain assumption was used. Analyses were performed for stiff and ductile adhesive types both analytically and numerically. In addition, a comparison of peak shear and peak peel stress values was carried out on the basis of percentage error. The results show that both analytical and numerical analyses were in very close agreement.

Key words: Single Lap Joint, Analytical Model, Finite Element Analysis

1. Introduction

Prediction of lap joint strength requires knowledge of stress distributions and magnitudes in the adhesive beyond proper failure criteria. Due to the wide application fields, single lap joints are used extensively to investigate the stress distributions and magnitudes along the bondline length. There are large numbers of studies used analytical and numerical methods as a way of determine stress distributions along the bondline length [1-8]. In most of these studies, two dimensional geometry and linear material properties are used to predict the stress distributions in analytical and numerical models.

Two dimensional geometry may be appropriate for single lap joints in which stress variations are acceptably small along the width direction. In addition, linear material assumption allows simplifying the solution of analytical model. However, if nonlinear materials properties must be used, the numerical analysis is then more practical method.

In this study, shear and peel stress distributions of single lap joints with stiff and ductile adhesives were investigated both analytically and numerically. In order to compare the analytical solutions with the numerical results, distributions of the same stress components obtained both methods were plotted in the same figure. In addition, a comparison of peak shear and peak peel stress values was carried out on the basis of percentage error.

*Corresponding author: Address: Industrial Design Engineering, Faculty of Technology, Karabuk University, Balıklarkayası mevkii, 78050, Karabuk, Turkey. E-mail address: ooz@karabuk.edu.tr, Phone: +905053941480

2. Analytical Model

A recent study on analytical modeling of single lap joint has been made by Zhao [9]. He proposed some closed-form solutions to evaluate the stress components along the adhesive bondline and then extended these solutions to the variable adhesive bondline by taking into account the bending effect [10]. This model also can be used to obtain the distribution of the normal, shear and peel stress components along the bondline for both lap joints with variable and single adhesive bondlines. Adhesive bondline can be modeled as three individual regions according to their shear modulus components (Figure 1) [10].

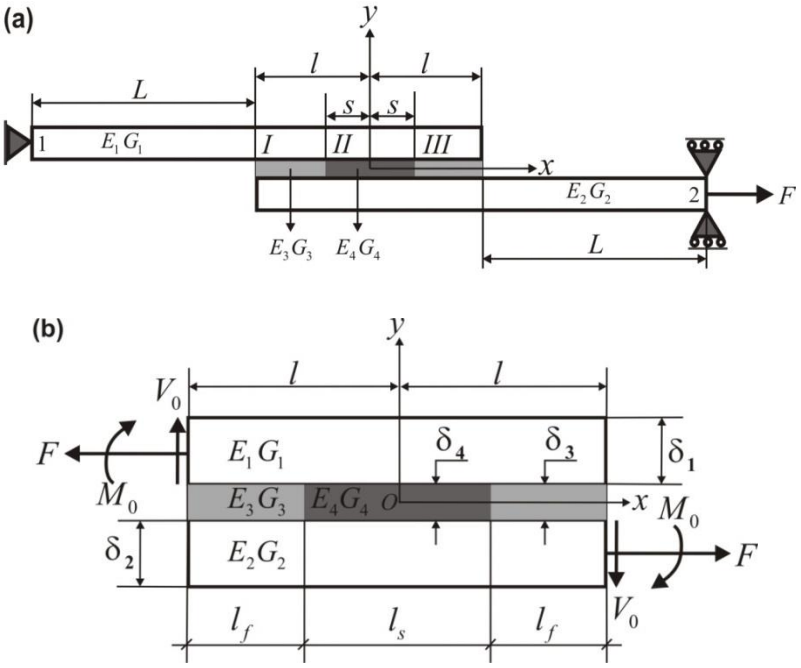

Figure 1. Bi-adhesive single lap joint under a tensile load: (a) geometric and material parameters, (b) force equilibrium free-body diagram [10]

The stiff adhesive was located in the middle and flexible adhesive at the ends of the overlap. Two adherends with the thicknesses of δ_1 and δ_2 were bonded with a graded adhesive layer with a thickness of δ_3, where $\delta_3 = \delta_4$. The region I and III at the overlap ends are the left and right flexible adhesive regions, respectively. The region II at the center of the overlap is the stiff adhesive region. Two ends of the adherends are simply supported, and the right end is subjected to an axial force F [10].

In Figure 1, l_f is the flexible adhesive length and l_s is the stiff adhesive length. Here, $l_f = (l - s)$ and $l_s = 2s$. The upper and the lower adherends are denoted by the subscripts 1 and 2, respectively. The flexible and stiff adhesives are denoted by the subscripts 3 and 4, respectively. Then, E_i and G_i $(i = 1, 2, 3, 4)$ are the modulus of elasticity and shear of the four individual components. The total overlap length is 2ℓ. The joint width, perpendicular to the (x, y)-plane, is

b. V_0 and M_0 are the shear force and bending moment acting on the ends of the upper and lower adherends, respectively (Figure 1(b)). A differential section dx can be cut out from the overlap region of the bi-adhesive joint as shown in Figure 2[10].

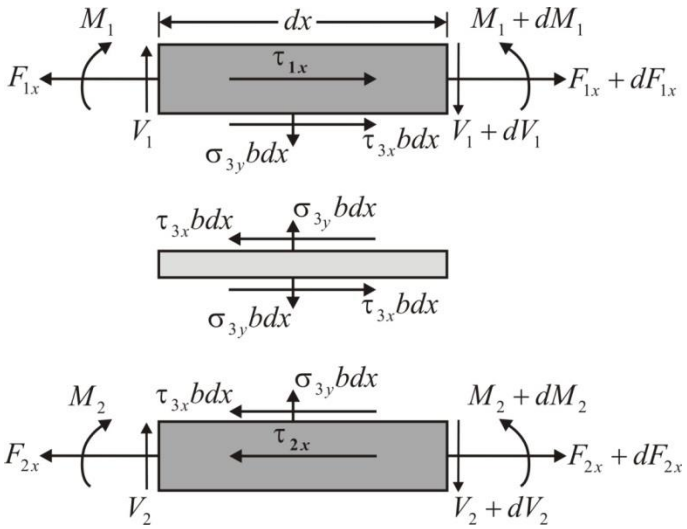

Figure 2. Free-body force equilibrium diagram [10]

where σ_{3y} is the peel stress at the upper and lower interfaces of the flexible adhesive. F_{ix}, V_i and M_i $(i = 1,2)$ are the tensile forces, shear forces and bending moments related to the upper and lower adherends, respectively. The distributions of the longitudinal shear stresses and displacements of adherend 1 and 2 are illustrated in Figure 3. The analytical model was based on the plane elasticity assumptions. A linear shear stress and strain distributions through the thickness of the adherends are assumed [10].

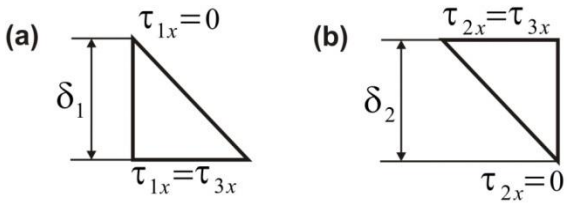

Figure 3. Longitudinal shear stress and displacement distributions through the thickness of the adherends ; (a) upper adherend, (b) lower adherend [10]

For the three regions (I, II and III) shown in Figure 1, the three sets of stress expressions are given as follows [10]

Region I ($-l \le x \le -s$)

$$\sigma_{1x}^{I} = A_1 \sinh(\lambda_1 x) + A_2 \cosh(\lambda_1 x) + A_3 x + A_4$$

$$\tau_{3x}^{I} = -\delta_0 (A_1\lambda_1 \cosh(\lambda_1 x) + A_2\lambda_1 \sinh(\lambda_1 x) + A_3) \qquad (1a)$$

$$\sigma_{3y}^{I} = B_1 \sinh(\omega_1 x)\sin(\omega_1 x) + B_2 \sinh(\omega_1 x)\cos(\omega_1 x) + B_3 \cosh(\omega_1 x)\sin(\omega_1 x) + B_4 \cosh(\omega_1 x)\cos(\omega_1 x)$$

Region II ($-s \le x \le s$)

$$\sigma_{1x}^{II} = A_5 \sinh(\lambda_2 x) + A_6 \cosh(\lambda_2 x) + A_7 x + A_8$$

$$\tau_{4x}^{II} = -\delta_0 (A_5\lambda_2 \cosh(\lambda_2 x) + A_6\lambda_2 \sinh(\lambda_2 x) + A_7) \qquad (1b)$$

$$\sigma_{4y}^{II} = B_5 \sinh(\omega_2 x)\sin(\omega_2 x) + B_6 \sinh(\omega_2 x)\cos(\omega_2 x) + B_7 \cosh(\omega_2 x)\sin(\omega_2 x) + B_8 \cosh(\omega_2 x)\cos(\omega_2 x)$$

Region III ($s \le x \le l$)

$$\sigma_{1x}^{III} = A_9 \sinh(\lambda_1 x) + A_{10} \cosh(\lambda_1 x) + A_{11} x + A_{12}$$

$$\tau_{3x}^{III} = -\delta_0 (A_9\lambda_1 \cosh(\lambda_1 x) + A_{10}\lambda_1 \sinh(\lambda_1 x) + A_{11}) \qquad (1c)$$

$$\sigma_{3y}^{III} = B_9 \sinh(\omega_1 x)\sin(\omega_1 x) + B_{10} \sinh(\omega_1 x)\cos(\omega_1 x) + B_{11} \cosh(\omega_1 x)\sin(\omega_1 x) + B_{12} \cosh(\omega_1 x)\cos(\omega_1 x)$$

The superscripts I, II and III denote the relevant stress components of the three individual regions (see Figure 1). σ_{1x} is the longitudinal normal stress of the adherends. σ_{iy} and τ_{ix} ($i = 3,4$) are the peel and shear stresses along the adhesive mid-plane. Equations (1a) and (1c) are related to the right and left flexible adhesive region. Equation (1b) is related to the stiff adhesive region, the central region. In Equation (1), there is a total of 24 unknown coefficients corresponding to the three regions. The 24 unknown coefficients can be obtained from the set of boundary conditions. Normal, shear and peel stresses can be evaluated by using the appropriate expressions for each region. As seen in Figure 1, the x-axis passes through the mid-plane of the adhesive layer. Therefore, analytical expressions are related to the mid-plane of the adhesive layer [10]. The detailed stress component derivations for the bi-adhesive joint was given by Özer and Öz [10].

Equations (1a-c) give distribution of stress components of single adhesive lap joint with the assumption of $\lambda_1 = \lambda_2$ and $\omega_1 = \omega_2$.

3. Finite element model

Numerical analyses were performed by two-dimensional finite element model. Linear material properties were used and the solutions were obtained by the assumption of plane strain condition. Both adherends and adhesive were meshed with plain strain elements (CPE4R). Figure 4 shows

the boundary conditions of single lap joint used in numerical analysis.

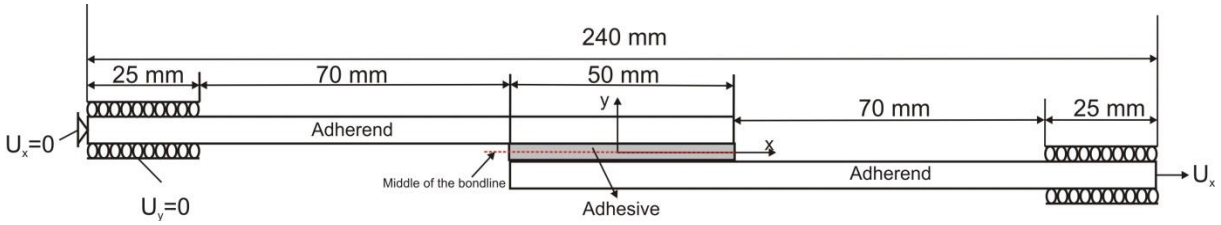

Figure 4. Boundary conditions of single lap joint

4. Materials

4.1 Adherend

DIN C75 hard steel was used as adherend. Table 1 shows the adherend mechanical properties.

Table 1. Adherend mechanical properties [11]

Modulus of elasticity (MPa)	**Poisson's ratio**	**Tensile strength** (MPa)	**Tensile yield strength** (MPa)
198300	0.29	1413	1260

4.1 Adhesives

In the analytical and numerical models, two adhesives with different characteristics were selected in order to be used in single lap joints. The adhesives used were identified as stiff (AV138) and ductile (Araldite 2015) based on their characteristics. Mechanical properties of adhesives were given in Table 2.

Table 2. Mechanical properties of Adhesives [11,12-14]

		Adhesives	
Trade name		Araldite 2015	Araldite AV138 M
Elasticity modulus	MPa	1850±0.21	4590±0.81
Poisson's ratio		0.33	0.35
Tensile strength	MPa	21.63±1.61	41.01±7.28
Tensile yield strength	MPa	12.63±0.61	36.49±2.47
Shear modulus	MPa	560±0.21	1560±0.01
Shear yield strength	MPa	14.6±1.3	25.1±0.33
Shear strength	MPa	17.9±1.8	30.2±0.4
Shear failure strain	%	43.9±3.4	7.8±0.7

3. Results and Discussion

In this section, distributions of the shear stress (τ_{xy}) and peel stress (σ_y) at the middle of the adhesive thickness were plotted along the adhesive bondlines. Experimental failure loads were

applied to numerical and analytical models. The experimental failure loads of the AV138 and Araldite 2015 adhesive joints are 14.51 kN and 20.76 kN, respectively [15]. Comparisons between the peak stress values were carried out on the basis of the percent error. Percentage error is defined as follows:

$$Error\,\% = \frac{Numeric - Analytic}{Numeric} x100 \qquad (1)$$

Figures 5and 6 show the shear stress distributions of AV138 and Araldite 2015 adhesive joints along the middle of the adhesive, respectively. As can be seen in Figures 5 and 6, analytical solution shows a good agreement with numerical one. At the edges of joint, numerical model tries to model the zero stress state. In analytical model, the zero stress state condition was not considered, so that peak shear stresses are always at the ends.

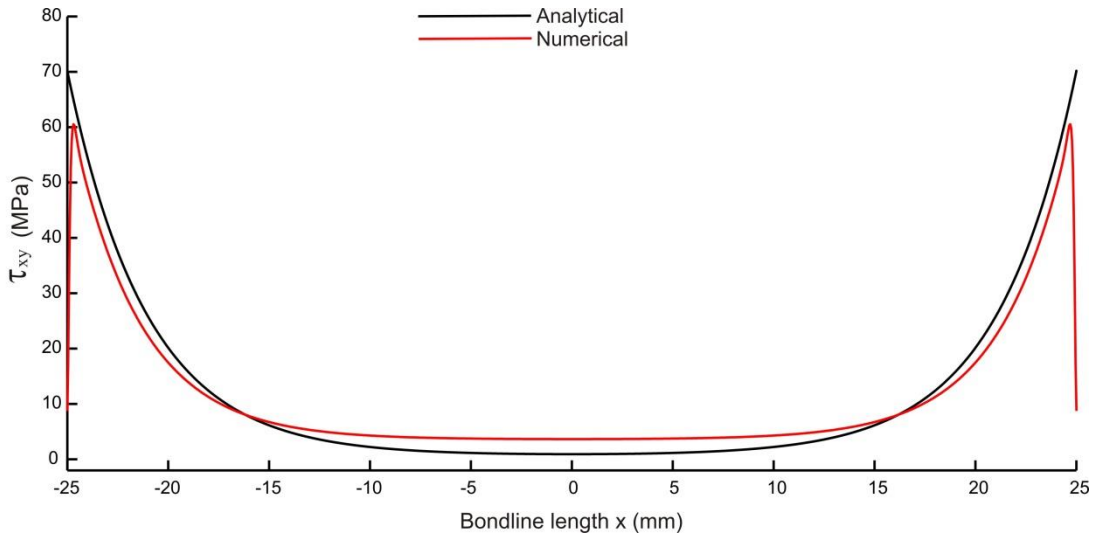

Figure 5. Shear stress distribution at the middle of the adhesive for AV138 adhesive joint

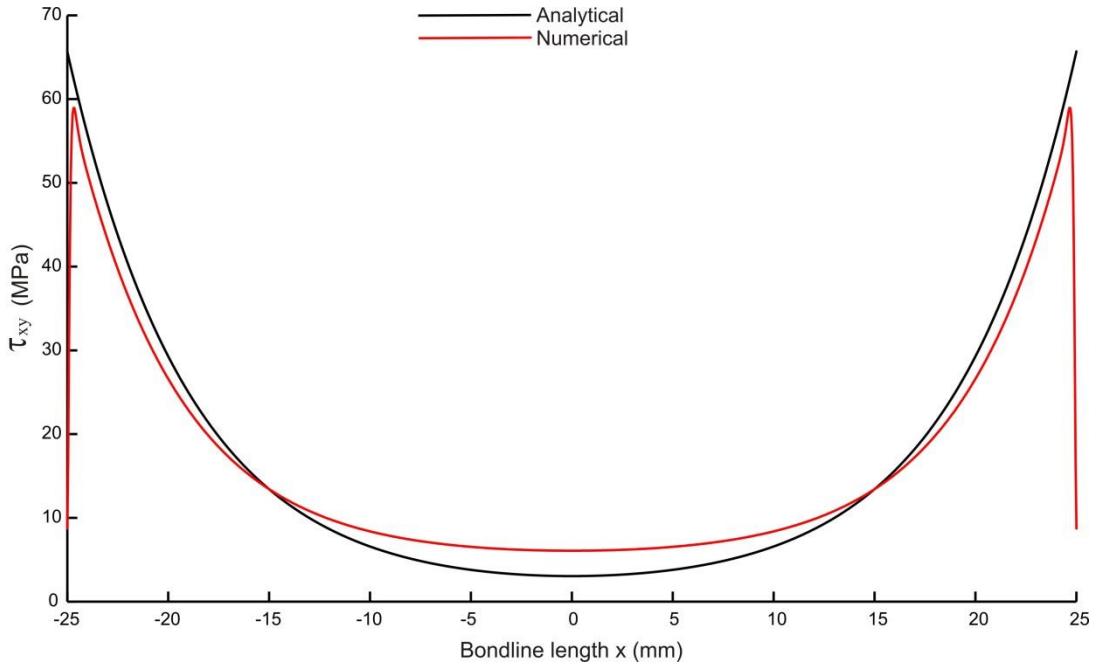

Figure 6. Shear stress distribution at the middle of the adhesive for Araldite 2015 adhesive joint

It can be seen from Figure 5 that the shear stress distributions is not uniform. This can be explained by the bending moment effect that cause peel stresses at the ends. Applied load mainly transfers at the ends and contribution of the middle part of the adhesives to load carrying is lower than the ends. However, for the Araldite 2015 adhesive, contribution of the middle part of the adhesive to load carrying is higher than that of AV138 adhesive joint. This is because the Araldite 2015 adhesive is ductile and has high deformation capacity. Apparent difference about the results for the adhesive joints is that analytical results show a higher shear stress compared to the peak values of the numerical results (Figures 5 and 6). As compared the analytical peak shear stresses with numerical ones, numerical results underestimate the shear stresses related to AV138 and Araldite 2015 adhesive joints with percent difference of 15.95% and 11.44%, respectively. Shear strengths of AV138 and Araldite2015 adhesive bulk specimens are 25.1 MPa and 14.6 MPa, respectively (see Table 2). It is seen in Figures 5 and 6 that, at the overlap edges, peak stresses exceed adhesives shear strengths under the experimental failure load levels.

Figures 7 and 8 show the peel stress distributions of AV138 and Araldite 2015 adhesive joints along the middle of the adhesive, respectively. For both adhesive joints, the analytical peel stress distributions coincide with those obtained from numerical analysis, except negative peel and end regions.

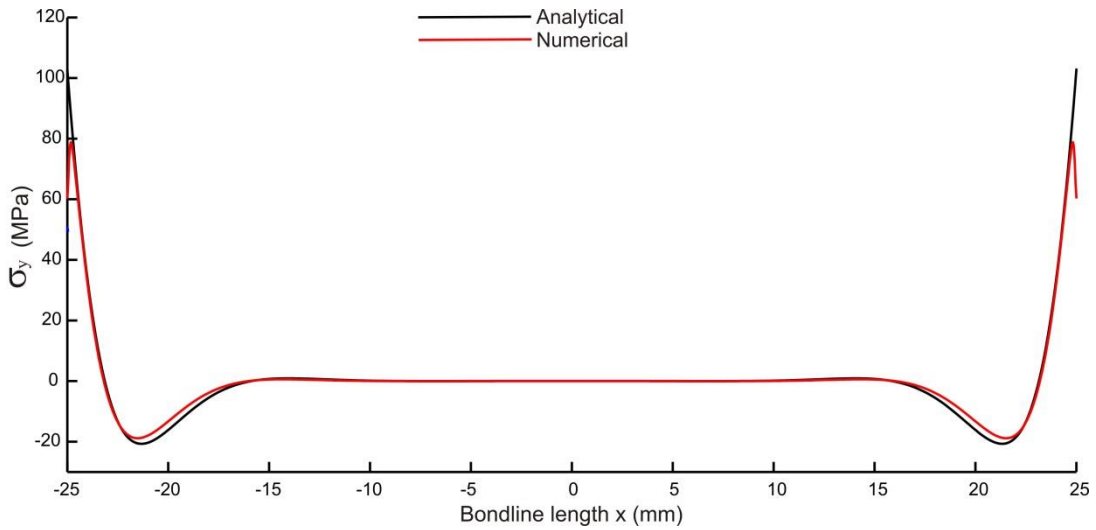

Figure 7. Peel stress distribution at the middle of the adhesive for AV138 adhesive joint

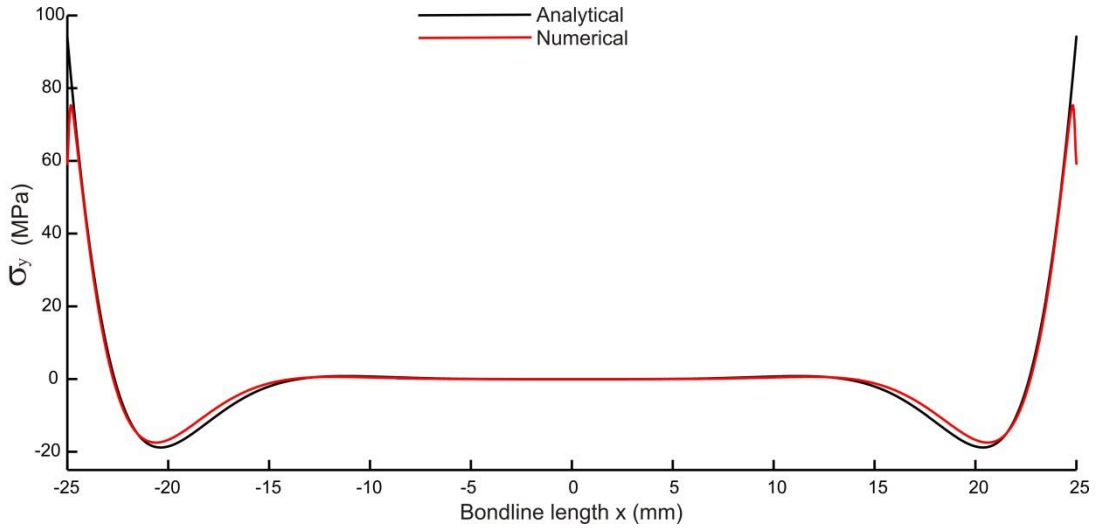

Figure 8. Peel stress distribution at the middle of the adhesive for Araldite 2015 adhesive joint

Analytical solution was not consider free edge condition, and then discrepancies between the analytical peel stresses and the numerical ones were observed at the ends. As compared the analytical peak peel stresses with numerical ones, numerical results underestimate the peel stresses related to AV138 and Araldite 2015 adhesive joints with percent difference of 30.57% and 25.17%, respectively. It should also be noted that the tensile strengths of AV138 and Araldite 2015 adhesive bulk specimens are 41.01 MPa and 21.63 MPa, respectively (see Table 2). It is seen in Figures 7 and 8 that, at the overlap edges, peak stresses exceed adhesives tensile strength under the experimental failure load levels.

Conclusions

In this study, shear and peel stress distributions of the single lap joints with different adhesives were investigated by analytically and numerically. In addition, a comparison between the peak values of numerical and analytical stress values was carried out on the basis of percentage error.

The main conclusions of this study can be summarized as following:

1- Shear distribution of Araldite 2015 adhesive joint is more uniform than that of AV138 adhesive joint. This is because the araldite 2015 adhesive has high deformation capacity and low stiffness. Apparent difference is that analytical results show a higher shear stress compared to the peak values of the numerical results. As compared the analytical peak shear stresses with numerical ones, numerical results underestimate the shear stresses related to AV138 and Araldite 2015 adhesive joints with percent difference of 15.95% and 11.44%, respectively.

2- The analytical peel stress distributions coincide with those obtained from numerical analysis, except for negative peel and end regions. As compared the analytical peak peel stresses with numerical ones, numerical results underestimate the peel stresses related to AV138 and Araldite 2015 adhesive joints with percent difference of 30.57% and 25.17%, respectively.

3- Peak shear and peak peel stress magnitudes of stiff and ductile adhesive obtained from both analytical and numerical models exceed the shear and tensile strengths of the adhesives. It can be concluded that linear analysis underestimates the joint strength.

References

[1] Adams RD, Peppiatt NA. Effect of Poisson's ratio strains in adherends on stresses of an idealized lap joint. J. Strain Anal. Eng. Des. 1973;8:134–139

[2] Hart-Smith LJ. Adhesive-bonded single-lap joints. NASA CR-112236;1973.

[3] Adams RD, Peppiatt NA. Stress analysis of adhesive-bonded lap joints. J. Strain Anal. Eng. Des. 1974;9:185–196.

[4] Allman DJ. A theory for elastic stresses in adhesive bonded lap joints. Q. J. Mech. Appl. Math. 1977;30:415–436.

[5] Bigwood DA, Crocombe AD. Elastic analysis and engineering design formulae for bonded joints. Int. J. Adhes. Adhes. 1989;9:229–242.

[6] Tsai MY, Oplinger DW, Morton J. Improved theoretical solutions for adhesive lap joints. Int. J. Solids Struct. 1998;35:1163–1185.

[7] Zhao B, Lu Z-H. A two-dimensional approach of single-lap adhesive bonded joints. Mech. Adv. Mater. Struct. 2009;16:130–159.

[8] Zhao B, Lu Z-H, Lu Y-N. Closed-form solutions for elastic stress–strain analysis in unbalanced adhesive single-lap joints considering adherend deformations and bond thickness. Int. J. Adhes. Adhes. 2011;31:434–445.

[9] Zhao B. Theoretical stress model of mixed-modulus single-lap adhesive bonded joints considering the bending effect. Chinese Journal of Mechanical Engineering. 2008; 44: 129–137.

[10] Özer H, Öz Ö. A comparative evaluation of numerical and analytical solutions to the bi-adhesive single-lap joint. Math. Probl. Eng. 2014; Article ID 852872: 1–16.

[11] da Silva LFM, Lopes MCQ. Joint strength optimization by the mixed-adhesive technique, Int. J. Adhes. Adhes. 2009;29:509–514.

[12] da Silva LFM, Rodrigues TNSS, Figueiredo MAV, De Moura MFSF. Chousal JAG. Effect of Adhesive Type and Thickness on the Lap Shear Strength. J. Adhes. 2006;82: 1091–1115.

[13] Pinto AMG, Campilho RDSG, Mendes IR, Baptista APM. "Numerical and Experimental Analysis of Balanced and Unbalanced Adhesive Single-Lap Joints between Aluminium Adherends. J. Adhes. 2014; 90: 89–103.

[14] Pinto AMG, Magalhães AG, Campilho RDSG, De Moura MFSF, Baptista APM. Single-Lap Joints of Similar and Dissimilar Adherends Bonded with an Acrylic Adhesive. J. Adhes. 2009; 85: 351–376.

[15] Öz, Ö. Hibrit Yapıştırma Bağlantı Hasarının Numerik ve Deneysel Olarak İncelenmesi. PhD Thesis, Yıldız Teknik Üniversitesi, İstanbul, 2015.